Carina's defiant Finger: *HST* observations of a photoevaporating globule in NGC 3372*

Nathan Smith,[1]†‡§ Rodolfo H. Barbá[2] and Nolan R. Walborn[3]

[1]*Center for Astrophysics and Space Astronomy, University of Colorado, 389 UCB, Boulder, CO 80309, USA*
[2]*Departamento de Física, Universidad de La Serena, Benavente 980, La Serena, Chile*
[3]*Space Telescope Science Institute, 3700 San Martin Drive, Baltimore, MD 21218, USA*

ABSTRACT

We present *Hubble Space Telescope* Wide Field Planetary Camera 2 images of a prominent externally ionized molecular globule in the Carina Nebula (NGC 3372), supplemented with ground-based infrared images and visual-wavelength spectra. This molecular globule has a shape resembling a human hand, with an extended finger that points toward its likely source of ionizing radiation. Following an analysis of the spatially resolved ionization structure and spectrum of the photoevaporative flow from the Finger, we conclude that the dominant ionizing source is either the WNL star WR25 (HD 93162), the adjacent O4 If-type star Tr16-244, or perhaps both. We estimate a mass-loss rate of $\sim 2 \times 10^{-5}\,\mathrm{M_\odot\,yr^{-1}}$ from the main evaporating surface of the globule, suggesting a remaining lifetime of $10^{5.3}$–10^6 yr. We find a total mass for the entire globule of more than $6\,\mathrm{M_\odot}$, in agreement with previous estimates. The hydrogen column density through the globule derived from extinction measurements is a few times $10^{22}\ \mathrm{cm^{-2}}$, so the photodissociation region behind the ionization front should be limited to a thin layer compared to the size of the globule, in agreement with the morphology seen in H_2 images. Although a few reddened stars are seen within the boundary of the globule in near-infrared continuum images, these may be background stars. We do not detect a reddened star at the apex of the finger, for example, down to a limiting magnitude of $m_K \simeq 17$. However, considering the physical properties of the globule and the advancing ionization front, it appears that future star formation is likely in the Finger globule, induced by radiation-driven implosion.

Key words: stars: formation – ISM: globules – H II regions – ISM: individual: NGC 3372.

1 INTRODUCTION

Compact bright-rimmed molecular globules are common in evolved massive star-forming regions, and are among the last vestiges of the molecular cloud that gave birth to the OB stars powering the H II region (e.g. Bok & Reilly 1947). These globules are externally illuminated and are photoevaporated and photoionized by ultraviolet (UV) radiation. They typically range in size from 0.1 to 1 pc, and appear striking in [S II] $\lambda\lambda$6717,6731 and Hα emission arising in the limb-brightened surfaces of their thin ionization fronts. Famous examples of this class of objects are Thackeray's globules in IC 2944

(Thackeray 1950; Reipurth, Raga & Heathcote 2003), as well as similar features in the Rosette Nebula (Herbig 1974), the Gum Nebula (Hawarden & Brand 1976; Reipurth 1983), and the Carina Nebula (Walborn 1975; Cox & Bronfman 1995).

Material evaporated from these clumps partly fills the interior of an H II region and may help stall the advance of the main ionization front by absorbing incident Lyman continuum radiation and converting it to a recombination front, but perhaps the most pertinent role played by these globules is that they are potential sites of continued star formation. Some globules show clear evidence for embedded star formation, while others do not (Reipurth 1983; Reipurth et al. 2003). If they are sites of star formation, one possibility is that they are simply dense cores that spontaneously collapsed to form stars and were then uncovered by the advancing ionization front. Another more intriguing idea is that pressure from the ionization shock front at the surface propagates through a globule and helps to overcome the magnetic, turbulent and thermal pressure that supports it against collapse, thereby inducing a star to form in the globule. This process of radiation-driven implosion is often referred to as *triggered star formation*. However, direct and unambiguous observational evidence for actively triggered star formation remains

elusive; the pillars in M16 may be an example of this phenomenon (Hester et al. 1996; White et al. 1999; Williams, Ward-Thompson & Whitworth 2001; McCaughrean & Andersen 2002). Numerous investigators have examined theoretical aspects of these evaporating globules, including details of the photoevaporative flows, their effect on the surrounding H II region, the shaping, destruction and acceleration of the globule (through the 'rocket effect'), and the possibility of triggered collapse and star formation due to the pressure of the impinging ionization front (Oort & Spitzer 1955; Kahn 1969; Dyson 1973; Elmegreen 1976; Bertoldi 1989; Bertoldi & McKee 1990; Dyson et al. 1995; Bertoldi & Draine 1996; Lizano et al. 1996; Williams 1999; Williams et al. 2001; Gorti & Hollenbach 2002). The evolution of these globules depends strongly on the incident UV radiation field, the initial size and density of the globule, and other properties, so observations of them in a wide variety of different environments are useful.

A rich population of these globules resides in the Carina Nebula (NGC 3372; $d = 2.3$ kpc), with the most notable grouping clustered around the famous Keyhole Nebula. Their emission from ionized, photodissociated, and molecular gas has been documented by several studies (Deharveng & Maucherat 1975; Walborn 1975; Cox & Bronfman 1995; Brooks et al. 2000; Rathborne et al. 2002; Smith 2002). There are a dozen of these clumps around the Keyhole, with typical masses of order 10 $M_\odot$ (Cox & Bronfman 1995). A few of these are seen only in silhouette, but most have bright H_2 and poly-

cyclic aromatic hydrocarbon (PAH) emission from their illuminated surfaces (Brooks et al. 2000; Rathborne et al. 2002). In addition, several dozen smaller features with diameters of only ∼5000 au were recently discovered by Smith, Bally & Morse (2003a), and additional proplyd candidates are seen in our images (see below, and Barbá et al. in preparation). They may be either large photoevaporating circumstellar discs (proplyds) or very small cometary clouds that are remnants of larger globules in more advanced stages of photoevaporation (e.g. Bertoldi & McKee 1990). It is not yet known if these smaller proplyd candidates or the larger globules in Carina contain embedded protostars or collapsing cores that may someday form stars. However, one large globule in the southern part of the nebula has recently been shown to harbour a Class I protostar that drives the HH 666 jet (Smith, Bally & Brooks 2004). In any case, these globules present a rare opportunity to study their associated phenomena in an environment powered by some of the hottest and most massive stars in the Galaxy (Walborn 1995; Walborn et al. 2002), while still being located near to us and suffering little interstellar extinction.

In this paper we undertake a detailed analysis of one particularly striking bright-rimmed globule in the Carina Nebula (see Fig. 1) that we call the 'Finger' because of its gesticulatory morphology (it has previously been identified as clump 4; Cox & Bronfman 1995). The defiant finger seems to point toward its dominant UV source, and as such, allows for an interesting application of models of
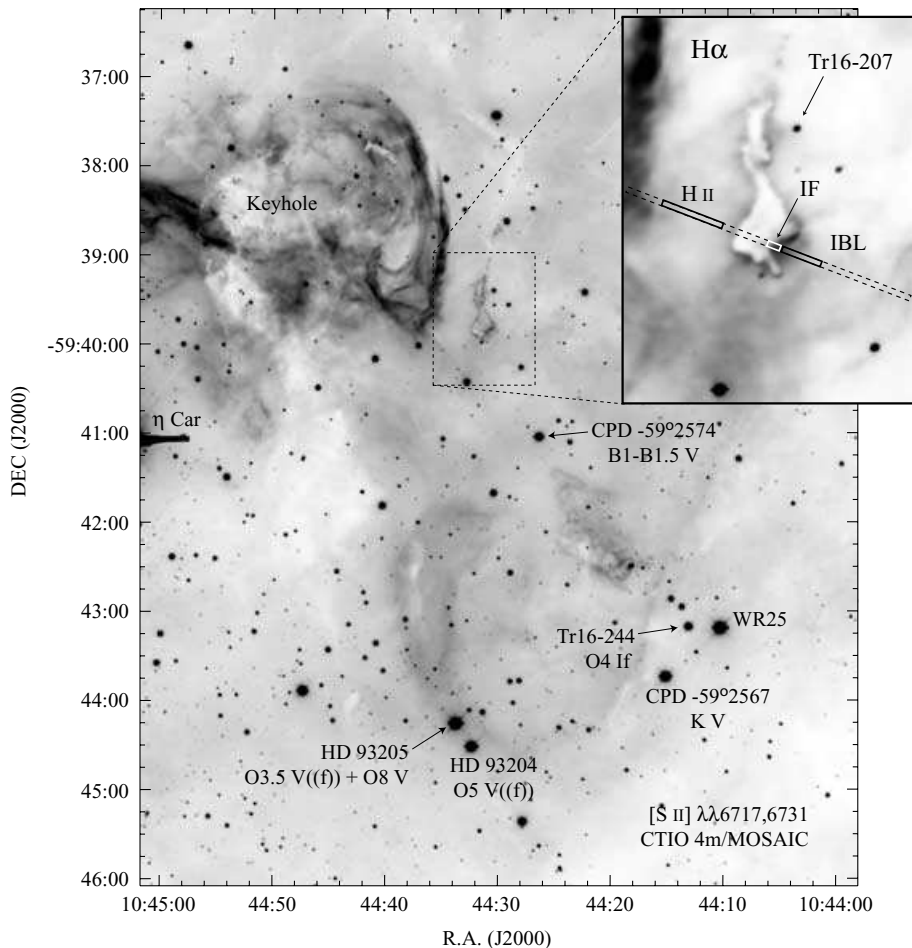

Figure 1. Large-scale image of the environment around the Finger, including the Keyhole and the background Carina nebula, η Car, WR25 and other stars. The [S II] image shown here was obtained with the MOSAIC camera on the CTIO 4-m telescope. The inset shows an enlargement of the Finger in the Hα filter, along with the orientation of the slit apertures used for spectra in Fig. 5.

Table 1. Observations of the Finger.

Telescope	Instrument	Filter or Emission lines	Exp. Time (s)	Comment
HST	WFPC2	F502N, [O III] λ5007	320	Image
HST	WFPC2	F656N, Hα, [N II]	400	Image
HST	WFPC2	F673N, [S II] $\lambda\lambda$6717,6731	800	Image
CTIO 4 m	OSIRIS	J	120	Image
CTIO 4 m	OSIRIS	H	120	Image
CTIO 4 m	OSIRIS	K	120	Image
CTIO 4 m	OSIRIS	He I λ10830	720	Image
CTIO 4 m	OSIRIS	Paβ	720	Image
CTIO 4 m	OSIRIS	H$_2$ 1-0 S(1) 2.122 μm	1080	Image
CTIO 1.5 m	RC Spec	blue; 3600–7100 Å	1200	Long-slit, PA = 69°
CTIO 1.5 m	RC Spec	red; 6250–9700 Å	1200	Long-slit, PA = 69°

photoevaporating globules mentioned above. In Section 2 we discuss our observations, and in Sections 3 and 4 we briefly discuss the results of our imaging and spectroscopy. In Section 5 we undertake a detailed analysis of the photoevaporative flow, and in Section 6 we discuss implications for potential star formation in the globule.

2 OBSERVATIONS AND DATA REDUCTION

2.1 *HST*/WFPC2 images

Images of the Keyhole Nebula were obtained on 1999 April 18 with the Wide Field Planetary Camera 2 (WFPC2) instrument onboard the *Hubble Space Telescope* (*HST*). Four different pointings were observed and combined to form a large mosaic image, which has been released by the Hubble Heritage Team.[1] Here we focus on only a small portion of the total area observed, containing the globule that we call the Finger. Images were obtained through narrowband filters F502N ([O III] λ5007), F656N (Hα) and F673N ([S II] $\lambda\lambda$6717,6731), as well as the broad-band filters F469W, F555W and F814W. Only the emission-line images will be discussed here, however. Pairs of images in each narrow-band filter were combined and processed in the usual way to remove cosmic rays and hot pixels, and to correct for geometric distortion, as described in the *HST Data Handbook*. Finally, the individual frames were combined to form a single mosaic image with a pixel scale of 0.0995 arcsec. The observations are summarized in Table 1, and subsections of the images showing the region around the Finger are displayed in Fig. 2, oriented with north up and east to the left.

2.2 Near-infrared images

Near-infrared (IR) images of the Finger and its immediate environment were obtained on 2003 February 25 with the Ohio State IR Imaging Spectrometer (OSIRIS) mounted on the CTIO 4-m telescope. OSIRIS has a 1024 × 1024 NICMOS3 array, with a pixel scale of 0.161 arcsec. Only a portion of the array is illuminated in this configuration, yielding a field of view of ∼1.5 arcmin. We obtained images in the broad-band *J*, *H* and *K* filters, as well as narrow-band filters isolating He I λ10830, Pa$\beta\lambda$12818 and H$_2$ 1-0 S(1) λ21218. In each filter, several individual exposures were taken with small offsets between them to correct for bad pixels on the array. The seeing during the observations was ∼0.8 arcsec. There

is no position on the sky near the Finger that is suitable for measuring the background sky because of bright emission from the H II region and nearby star clusters, so for sky subtraction we nodded the telescope to a position roughly 2° south. Flux calibration was accomplished by measuring isolated stars from the 2MASS catalog that were included in our field of view, and is valid to within about ±10 per cent. The IR images were aligned with the WFPC2 images and are shown in Fig. 3. Flux ratios of certain optical and IR images are shown in Fig. 4.

2.3 Optical spectroscopy

Low-resolution ($R \sim$ 700–1600) spectra from 3600 to 9700 Å were obtained on 2002 March 1 and 2 using the RC Spectrograph on the CTIO 1.5-m telescope. Long-slit spectra of the Finger were obtained with the 1.5-arcsec-wide slit aperture oriented at position angle (PA) ≈ 69° crossing through the middle of the globule as shown in Fig. 1. The pixel scale in the spatial direction was 1.3 arcsec. Spectra were obtained on two separate nights in two different wavelength ranges (blue, 3600–7100 Å; and red, 6250–9700 Å), with total exposure times and other details listed in Table 1. Sky conditions were mostly photometric, although a few thin transient clouds were present when the blue spectrum was obtained. Flux calibration and telluric absorption correction were accomplished using the standard stars LTT-3218 and LTT-2415.

From the resulting long-slit spectra, we extracted several one-dimensional (1D) segments of the slit that sampled emission from the thin ionization front (IF), the ionized boundary layer (IBL), the total emission from the IF and IBL (TOT), and a nearby sample of the emission from the background Carina Nebula H II region. The sizes of these subapertures are identified in Figs 1 and 5. The blue and red wavelength ranges of these extracted 1D spectra were merged to form a single 3600–9700 Å spectrum for each position, with a common dispersion of 2 Å pixel^{-1}; the average of the two was taken in the region of the spectrum near Hα where the blue and red spectra overlapped (in the overlap region, bright line fluxes agreed to within about ±5 per cent, comparable to the assumed uncertainty). Finally, the background H II region spectrum was subtracted from the IF, IBL and TOT spectra. The final flux-calibrated spectra are shown in Fig. 5. Observed intensities are listed in Table 2, relative to Hβ = 100. Uncertainties in these line intensities vary depending on the strength of the line and the measurement method. The integrated fluxes of isolated emission lines were measured; for these, brighter lines with $I > 10$ typically have measurement errors of a few per cent, and weaker lines may have uncertainties of ±10 to
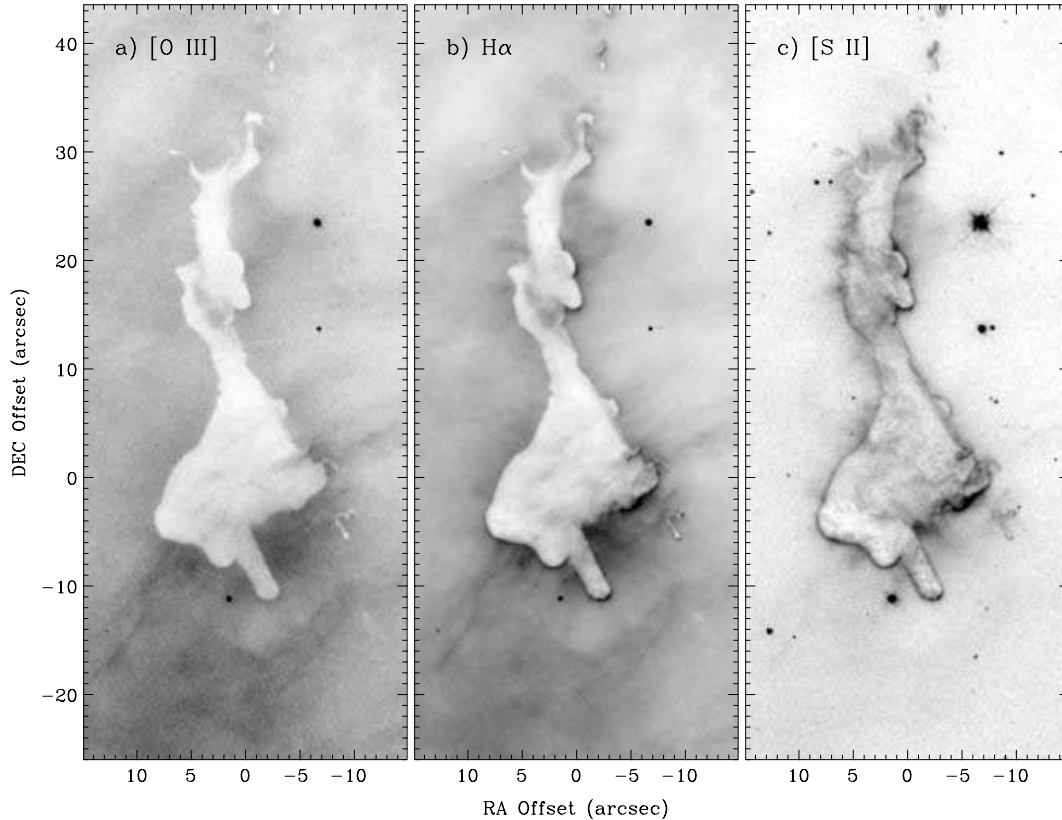
Figure 2. *HST*/WFPC2 images of the Finger. (a) F502N filter transmitting [O III] λ5007; grey-scale range from 2.4×10^{-14} (white) to 1.9×10^{-13} (black) ergs s^{-1} cm^{-2} arcsec^{-2}. (b) F656N filter transmitting Hα; grey-scale range from 5.4×10^{-14} (white) to 3×10^{-13} (black) ergs s^{-1} cm^{-2} arcsec^{-2}. (c) F673N filter transmitting [S II] λλ6717,6731; grey-scale range from 4.2×10^{-15} (white) to 3.3×10^{-14} (black) ergs s^{-1} cm^{-2} arcsec^{-2}. These observed flux levels were not corrected for reddening and extinction. The axes display offset in arcsec from an arbitrary central position in the globule.

15 per cent. The uncertainties increase somewhat at the blue edge of the spectrum. Blended pairs or groups of lines were measured by fitting Gaussian profiles. For brighter blended lines like Hα+[N II] and [S II], the measurement uncertainty is typically 5–10 per cent. Obviously, errors will be on the high end for faint lines adjacent to bright lines, and errors will be on the low end for the brightest lines in a pair or group, or lines in a pair with comparable intensity.

3 IMAGING RESULTS

Figs 2–4 show imaging data concentrated on a small region (less than 1 arcmin^2) featuring the evaporating molecular globule that is the focus of this paper. Images showing the Keyhole Nebula and its environment on a much larger spatial scale but with lower spatial resolution, and using filters transmitting these same optical and IR emission lines, have been presented by Deharveng & Maucherat (1975), Walborn (1975), López & Meaburn (1984), Brooks et al. (2000) and Smith (2002). Near-IR continuum images of the Finger will be discussed later in Section 6.

3.1 Emission-line morphology of the Finger

The overall morphology of the Finger in Figs 2 and 3 is quite striking, and consistent with the interpretation that the emission arises from the ionized evaporating flow and dense ionization fronts of an externally illuminated molecular globule. The [O III], Hα and [S II] images are reminiscent of many *HST*/WFPC2 images of dust pillars and globules in other H II regions (e.g. Hester et al. 1996; Reipurth

et al. 2003). Differences in the observed structure in various emission lines give interesting clues to the nature of the evaporating globule: In [O III] emission, the Finger is seen almost exclusively as a silhouette against the bright background, except for a faint halo from the evaporated flow around the globule. In Hα, the emission from the evaporating halo material and extinction features are almost identical to [O III], as the extended halo mostly disappears in the Hα÷[O III] image in Fig. 4(a). Hα is significantly stronger than [O III] only near the sharp limb-brightened edges of the cloud, where strong [S II] emission is also seen at the ionization front (i.e. the Hα÷[O III] flux ratio image in Fig. 4(a) looks nearly identical to the [S II] image). The globule itself appears to be optically thick, especially at visual wavelengths where it totally obscures the background H II region; the emission from [O III] and Hα seen projected within the boundaries of the globule is due primarily to the ionized evaporating flow on the near side. The globule does not become transparent at near-IR wavelengths like the pillars in M16 (e.g. Mc-Caughrean & Andersen 2002; Thompson, Smith & Hester 2002). It is seen clearly as a silhouette in Paβ, He I λ10830, Hα and [O III], but is not a silhouette in [S II] or H$_2$ because the emission from the front surface of the globule is brighter than the background. This is especially clear from the [S II]÷Hα ratio image in Fig. 4(b). The spatially resolved structure of the stratified ionization fronts and photoevaporating halo will be discussed in more detail in Section 5.

There appear to be two dominant locations of active photoevaporation where the surface of the globule is directly irradiated by individual stars; these are at the southern end of the globule (the 'knuckles', if the Finger globule is imagined to resemble a human
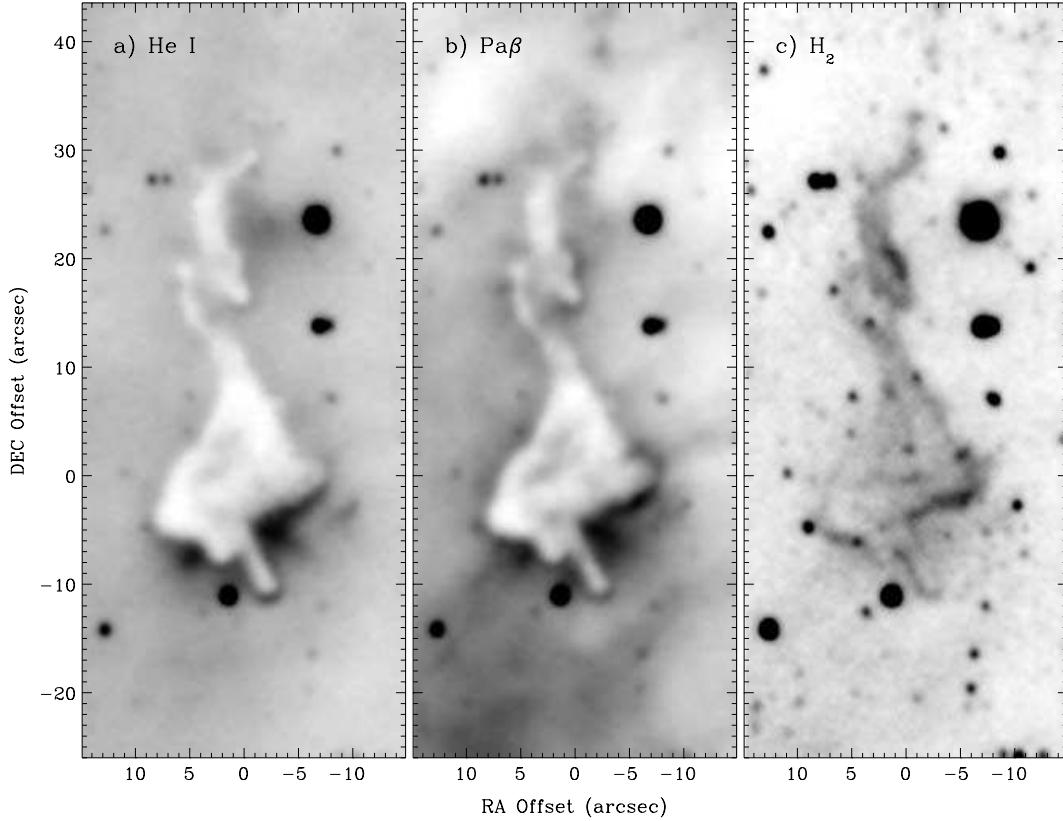
Figure 3. Near-IR images of the Finger. (a) He I $\lambda10830$; grey-scale range from 1.3×10^{-14} (white) to 4.8×10^{-14} (black) ergs s^{-1} cm^{-2} arcsec^{-2}. (b) Hydrogen Paβ; grey-scale range from 1.5×10^{-14} (white) to 5.1×10^{-14} (black) ergs s^{-1} cm^{-2} arcsec^{-2}. (c) H$_2$ $v = 1 - 0$ S(1) $\lambda21218$; grey-scale range from 9.3×10^{-16} (white) to 5.3×10^{-15} (black) ergs s^{-1} cm^{-2} arcsec^{-2}. These observed flux levels were not corrected for reddening and extinction.

hand), and at the western side of the northern part (the 'wrist'). The activity in these two regions is highlighted best by emission from He I $\lambda10830$ (Fig. 3a) and H$_2$ (Fig. 3c). The He I line has a metastable lower level and is enhanced by collisions in dense ionized gas, such as that found in a dense ionized photoevaporative flow. H$_2$ emission will be brightest in the photodissociation region (PDR) immediately behind the strongest ionization fronts, where a strong flux of FUV (Balmer continuum) photons penetrates, or where the gas is heated by a shock or Lyα from the ionization front itself. Both He I and H$_2$ are most prominent in the two regions mentioned above: the 'knuckles' and the 'wrist'. Relatively weak limb-brightened [S II] emission is seen around the periphery of the globule, probably caused by the ambient UV field and Lyα radiation.

The most obvious photoevaporating flow on the southern edge of the globule exhibits a thin straight finger protruding normal to a bright edge-on ionization front. This thin finger appears to identify its source of irradiation: it points toward PA $= 208°$, close to the massive star WR25 (HD 93162) at PA $= 219°$ relative to the Finger, although other early-type stars are seen along the same apparent trajectory. The ionizing source is addressed quantitatively in Section 5.2. Extending toward the south from this main ionization front is a large-scale ionized flow, prominent in [O III], Hα and Paβ, where it fills the lower left corner in Figs 2(a), (b) and 3(b). About 6 arcsec from the end of the finger, one can see an arc-shaped structure in these same emission lines; the density here might be enhanced in a shock as the ram pressure of the photoevaporating flow off the globule balances the pressure of the ambient ionized gas in the H II region. From conservation of momentum, this should occur at a distance from the centre of the globule given roughly by $r_{if}(n_{if}/n_{HII})^{0.5}$,

where n_{if} and n_{HII} are the electron densities at the ionization front and in the H II region, respectively, and r_{if} is the radius of curvature of the ionization front. Electron densities are estimated below (Table 3), and the resulting distance is in reasonable agreement with the location of the shock.

Both of the main evaporating surfaces of the globule are found at relatively flat interfaces (a large effective radius of curvature). This may be an important factor in their enhanced emission, as the radial density profile will fall off more rapidly in a spherically divergent flow than from a planar ionization front. The northern evaporative flow (the 'wrist') is particularly interesting, as it may be caused by a very nearby star – the bright B star located only 10 arcsec to the west (Tr16-207; see Fig. 1).[2] The motivation for this conjecture is that both the He I and H$_2$ emission are localized, while most of the rest of the western side of the globule also appears relatively flat and normal to the same direction. If the ionizing source were a luminous star at a large distance, we might expect to see a similar level of enhanced emission all along the western side of the globule. A third region of active photoevaporation may have a different UV source from the other two just mentioned; the south-east edge of the globule shows enhanced emission in [S II] and H$_2$, most notably on the east side of the thin finger, while such emission is not as strong on the west side of the same finger. The very luminous and massive evolved star η Carinae is located toward the south-east; η Car may

[2] Additionally, we note that the northern part of the globule appears to be curved with a radius of curvature of $\sim$10 arcsec, and with Tr16-207 located at the centre of curvature.
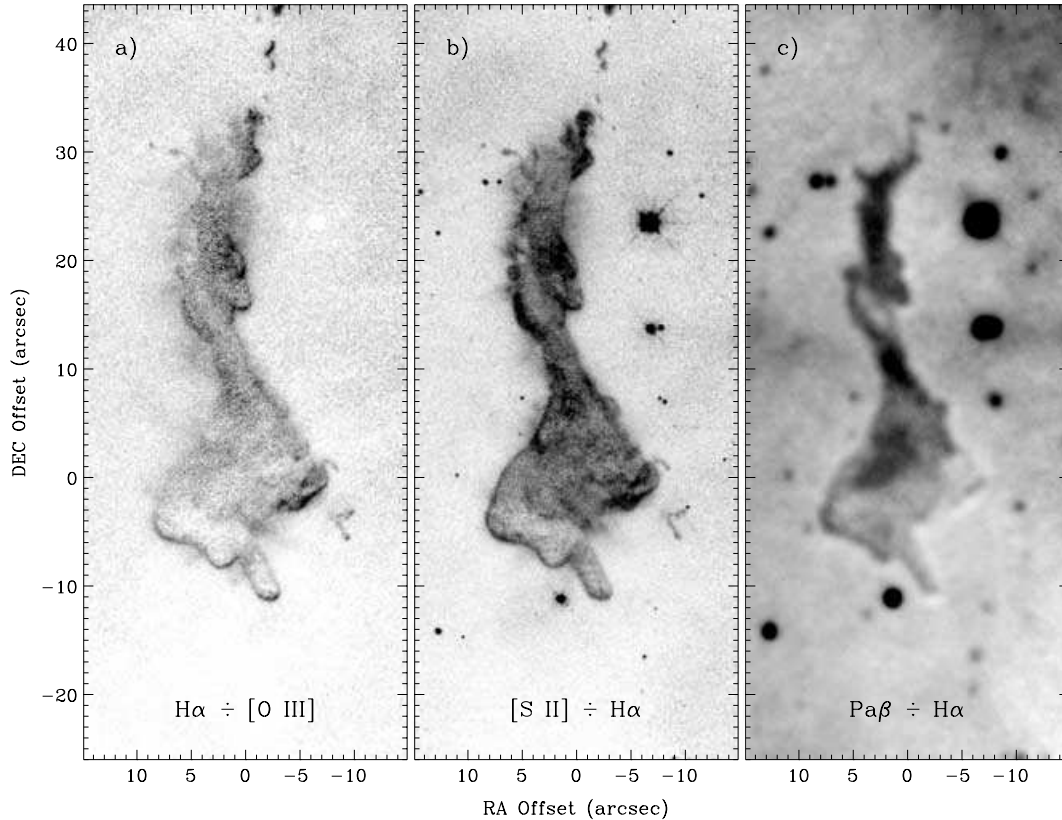
Figure 4. Selected flux-ratio images of the Finger. (a) Hα÷[O III] (F656N÷F502N) with the grey-scale range from 1 (white) to 2.3 (black). (b) [S II]÷Hα (F673N÷F656N) with the grey-scale range from 0.033 to 0.13. (c) The ground-based Paβ image divided by a smoothed *HST*/WFPC2 Hα image, with the grey-scale range from 0.07 to 0.12. Note that the F656N Hα image is partially contaminated by adjacent [N II] lines, which affects the value of the flux ratios listed here. These flux ratios have been corrected for reddening and extinction, using $E(B - V) = 0.37$ and $R = 4.8$ (see text).

have been a prodigious FUV source in the recent past (more than 160 yr ago) before it was surrounded by its young circumstellar dust shell (Smith, Gehrz & Krautter 1998). The O4 V((f+)) star HDE 303308 is seen toward the east/south-east as well, and may add to the FUV flux striking the side of the Finger.

3.2 Proplyd candidates?

The new *HST*/WFPC2 images also reveal a small group of distinct cometary clouds located immediately west of the Finger, the largest member of which has approximate dimensions of 0.5×2 arcsec^2 (about 1100×4500 au). This object closely resembles the numerous 'proplyd candidates' seen throughout the Carina Nebula (Smith et al. 2003a). This object, which we denote 104430.2–593953 (following the naming convention of Smith et al. 2003a), is smaller than many of the other cometary objects in Carina, but is still larger than the proplyds seen in Orion and is apparently seen primarily in extinction and limb-brightened emission from Hα and [S II]. The nature of these objects remains somewhat ambiguous (are they analogues of the proplyds of Orion, starless cometary clouds, or something in between?), but this image hints that an *HST* imaging survey of Carina would uncover many such objects that are missed in ground-based images.

4 SPECTROSCOPIC RESULTS

Fig. 5 shows ground-based spectra extracted from the long-slit data for subapertures identified in Fig. 1. The IF spectrum does not truly

isolate emission from the thin ionization front on the surface of the globule because these ground-based data lack the requisite spatial resolution. However, emission in this subaperture is dominated by the limb-brightened emission from the IF; this is especially true for low-ionization lines like [S II], whereas much of the emission in high-ionization lines like He I and [O III] may originate in immediately adjacent regions. The IBL spectrum samples the more extended photoevaporated flow, or the *ionized boundary layer* that absorbs the hard UV photons incident upon the globule. The TOT spectrum includes both the IF and the IBL, and is mainly useful for comparison with some diagnostic line ratios mentioned later. Finally, the background spectrum of the Carina Nebula is shown for comparison; of course, this is a mixture of the high-ionization gas inside the H II region with the ionization front and photodissociation regions on the far side of the nebula.

The most notable aspect of the IF spectrum is its low ionization, with strong [O II] λλ3726,3729, [N II] λλ6548,6583, and [S II] λλ6717,6731 compared to Hα. These lines are typically enhanced at the ionization front or just beyond it if they are not collisionally de-excited; O has roughly the same ionization potential as H, the ionization potential of S is below 13.6 eV, and although the ionization potential of N is 14.5 eV, it can be ionized from the excited ^{2}D state by photons with energies as low as 12.1 eV. The IBL spectrum is intermediate in ionization and excitation between the IF and the background H II region, as expected. The IF and IBL spectra qualitatively resemble the low- and high-excitation spectra, respectively, of the similar photoevaporating globule in the nearby open cluster NGC 3572 (Smith et al. 2003b).
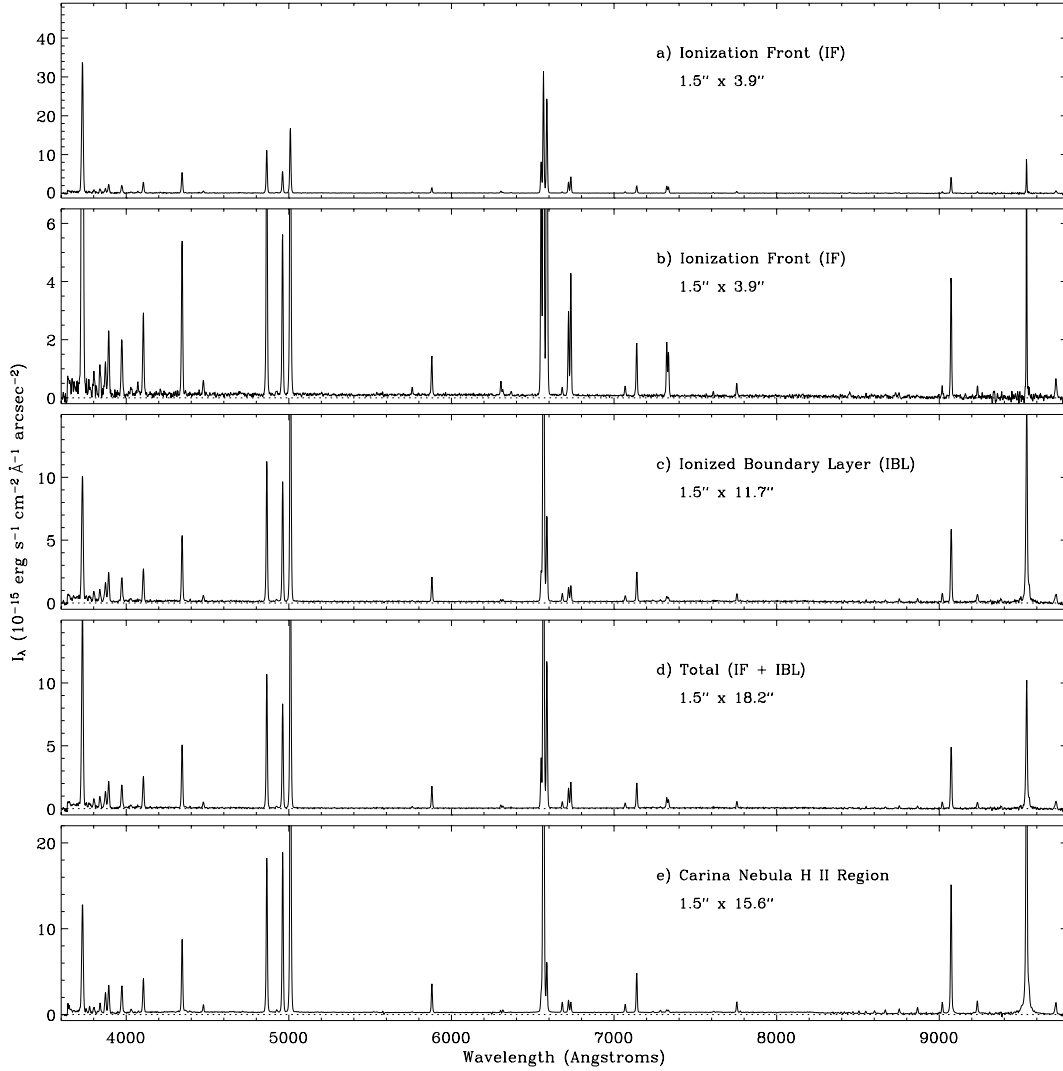
Figure 5. Spectra of gas associated with the Finger. The plotted quantity is the average specific intensity in the aperture size given in each panel, and shown in Fig. 1. (a) The spectrum of the ionization front (IF) on the side of the globule facing the main UV source. (b) Same as Panel *a* but with a different intensity scale. (c) Spectrum of the ionized boundary layer (IBL, or 'photoevaporative flow') associated with the main ionization front. (d) Spectrum of the total emission including both the ionization front and the ionized boundary layer (note that the 'total' emission shown here is not a simple average of the IF and IBL; the aperture used was slightly larger than both the IF and IBL combined; see Fig. 1). (e) Average spectrum of the background H II region near the Finger.

Table 2 lists observed and dereddened line intensities relative to H$\beta = 100$ for the various selected regions. The reddening used to correct the observed line intensities was determined by comparing observed strengths of hydrogen lines in the background H II region to the Case B values calculated by Hummer & Storey (1987). As shown in Fig. 6, the observed Balmer and Paschen decrements suggest a value for $E(B - V)$ of roughly 0.37 ± 0.03, using the reddening law of Cardelli, Clayton & Mathis (1989) with $R_V = A_V \div E(B - V) \approx 4.8$, which is appropriate for local extinction from dust clouds around the Keyhole Nebula (Smith 1987, 2002). The value of $E(B - V) = 0.37$ we derive from nebular emission is close to the average value of 0.47, and within the range of values of 0.25 to 0.64, as listed for several bright O-type stars in Tr16 by Walborn (1995). Table 3 lists representative physical quantities like electron density and temperature derived from a standard deductive nebular analysis of the usual line ratios. These are useful to guide the interpretation of the physics of the ionization front and photoevaporative flow discussed below.

5 ANALYSIS OF THE PHOTOEVAPORATIVE FLOW

Combining spectra with WFPC2 images that spatially resolve the stratified IF on the surface of the globule provides a powerful diagnostic tool, and allows us to undertake a detailed analysis of the photoevaporative flow and the incident UV field. From our narrow-band images we made tracings of the observed intensity normal to the IF at five different positions around the Finger, indicated as *a* through *e* in Fig. 7. The corresponding intensity tracings at these five positions are shown in Figs 8(a)–(e). Surface brightness in Fig. 8 has been corrected for reddening and extinction, with $E(B - V) = 0.37$ and $R = 4.8$.

5.1 The stratified ionization fronts of the Finger

All the tracings in Fig. 8 show the same general stratification with respect to the IF (at position $= 0$), although there are some detailed

Table 2. Observed and dereddened line intensities[a].

λ(Å) and ID	IF (Obs)	IF (Dered.)	IBL (Obs)	IBL (Dered.)	TOT (Obs)	TOT (Dered.)	H II (Obs)	H II (Dered.)
3727 [O II]	312	436	105	146	178	248	93.0	130
3869 [Ne III]	9.9	13.3	16.2	21.9	14.0	18.8	15.0	20.1
3889 H8+He I	19.1	25.5	22.2	29.7	21.7	29.0	20.2	27.1
3970 Hε+[Ne III]	18.1	23.7	19.2	25.2	20.0	26.2	20.6	27.1
4026 He I	2.9	3.7	2.4	3.1	2.4	3.1	2.6	3.3
4073 [S II]	3.9	5.0	...	...	1.6	2.0	0.7	1.0
4102 Hδ	24.8	31.3	23.4	29.6	23.8	30.0	23.4	29.5
4340 Hγ	44.6	52.6	46.3	54.7	47.5	56.1	44.9	53.0
4363 [O III]	0.8	0.9	1.3	1.6	0.8	0.9	4.9	5.7
4387 He I	...	...	0.9	1.1	0.8	0.9	0.5	0.6
4471 He I	4.1	4.7	4.3	4.9	4.5	5.1	4.9	5.6
4861 Hβ	100	100	100	100	100	100	100	100
4922 He I	1.6	1.6	1.5	1.5	1.3	1.3	1.6	1.5
4959 [O III]	51.7	50.1	83.8	81.2	77.1	74.7	99	96.1
5007 [O III]	161	153	254	242	236	225	300	286
5755 [N II]	3.22	2.5	0.8	0.6	1.5	1.2	0.7	0.56
5876 He I	15.0	11.2	16.3	12.2	15.8	11.8	16.8	12.5
6300 [O I]	5.1	3.4	1.3	0.9	2.2	1.5	0.9	0.6
6312 [S III]	2.5	1.7	1.4	0.9	1.6	1.1	1.4	1.0
6364 [O I]	1.8	1.2	0.6	0.4	0.8	0.5	0.3	0.2
6548 [N II]	95.1	61.2	29.1	18.7	41.8	26.9	19.2	12.4
6563 Hα	339	217	439	281	383	246	442	284
6583 [N II]	280	179	68.3	43.7	114	73.0	37.5	24.0
6678 He I	3.4	2.1	6.2	3.9	5.4	3.4	6.3	3.9
6717 [S II]	33.7	20.9	10.4	6.5	15.3	9.5	7.0	4.4
6731 [S II]	47.7	29.6	11.4	7.1	19.2	11.9	5.9	3.6
7065 He I	4.6	2.7	4.7	2.7	4.1	2.4	5.0	2.9
7136 [Ar III]	25.2	14.4	23.3	13.3	21.4	12.2	23.4	13.4
7237 [Ar IV]	...	...	1.2	0.7	...	...	0.9	0.5
7281 He I	...	...	1.1	0.6	...	...	1.3	0.7
7320 [O II]	22.5	12.4	4.0	2.2	7.6	4.2	1.5	0.8
7330 [O II]	20.4	11.2	3.1	1.7	6.7	3.6	1.3	0.7
7751 [Ar III]	6.6	3.3	5.9	3.0	5.8	2.9	6.2	3.1
7774 O I	...	...	0.6	0.3	...	...	0.6	0.3
8446 O I	3.9	1.7	...	...	...	...	1.1	0.5
8750 Pa12	2.4	1.0	2.6	1.1	2.3	1.0	3.4	1.4
8863 Pa11	3.4	1.4	3.0	1.2	2.5	1.0	4.0	1.6
9015 Pa10	7.2	2.8	7.2	2.8	6.0	2.3	6.5	2.6
9069 [S III]	68.1	26.6	66.3	25.9	59.4	23.2	86.9	34.0
9229 Pa9	6.9	2.6	7.2	2.7	5.8	2.2	7.6	2.9
9532 [S III]+Pa8	219[b]	79.7[b]	215	78.5	145	52.8	300	110
9711 [Fe II]	16.1	5.7	13.2	4.7	12.4	4.4	9.3	3.3

[a]Observed line intensities were dereddened using the extinction law of Cardelli et al. (1989), with $E(B - V) = 0.37$ and $R_V = 4.8$.
[b]The intensity of [S III] λ9532 was assumed to be 3×[S III] λ9069 in the IF spectrum, since that line at that position partly fell on a bad pixel on the detector.

differences. Starting from the left, H_2 emission peaks 0.5–1.5 arcsec (1200–3500 au at $d = 2.3$ kpc) behind the IF, while [S II], Hα and Paβ then rise sharply. [S II] peaks at the IF and decreases exponentially thereafter, while hydrogen lines continue to rise, with their peak ≲0.25 arcsec outside the IF in most cases (except position *b*). [O III] and He I rise sharply at the IF (due to extinction by dust), reach a broad peak (if any) outside the IF, and then decrease gradually at larger distances. The narrowest [S II] zones with a full width at half maximum (FWHM) of ∼0.5 arcsec are spatially resolved by *HST*, but the widths of some of the narrow Paβ and He I zones are unresolved in the ground-based images.

Far from the IF (∼7 arcsec) the intensities of Hα and [O III] are roughly equal in each set of tracings. Then, moving toward the IF, the intensities of Hα and [O III] diverge as hard photons capable of ionizing O^+ to O^{2+} (with $h\nu > 35$ eV) are eaten up by the photo-

evaporating flow and O^{2+} recombines (note the very strong [O II] λλ3727,3729 at the IF in Fig. 5 and Table 2). At the same time, the strength of [S II] tends to increase in proportion to the difference between Hα and [O III]. This is consistent with the qualitative similarity between the [S II] image (Fig. 2c) and the [O III]÷Hα ratio (Fig. 4a). Although every position shares the same basic behaviour described above, there are differences among the five positions. In particular, the IFs of *a* and *d* are much narrower than the other positions. The stratification at position *b* is particularly broad. These differences are probably due to different radii of curvature (although position B may be affected by evaporation off the near side of the thin finger as well). For example, at *b* the IF appears nearly straight, in stark contrast to the small radius of curvature at the end of the finger at position *a*. In general, a smaller radius of curvature means that the photoevaporative flow diverges and the density drops faster than
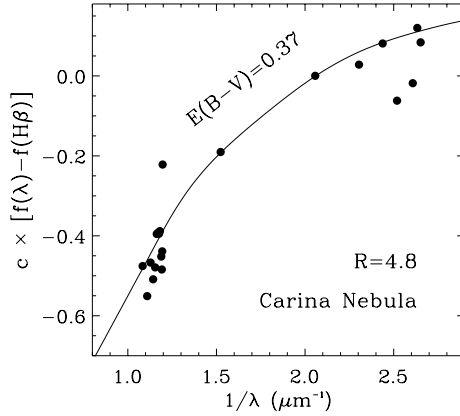
Figure 6. Observed reddening for hydrogen lines in the background Carina Nebula H II region near the Finger, relative to Hβ (dots). The solid curve shows the reddening for $E(B - V) = 0.37$ or a logarithmic extinction at Hβ of $c \simeq 0.83$ (assuming the ratio of total to selective extinction is $R_V = 4.8$).

in a planar IF, so the stratified ionization structure is compressed. Both positions b and e seem to be nearly planar surfaces with a high-density flow extending far from the IF.

5.2 Does WR 25 ionize the Finger?

As noted earlier, the finger at the southern end of the globule seems to point toward the luminous WNL star WR25 (HD 93162), but since some other luminous early-type stars are seen along this same general trajectory, this relationship should be tested quantitatively. By examining the properties of the IF and photoevaporative flow from the globule, we can estimate the necessary ionizing photon flux and the shape of the incident continuum. These can then be compared to likely values for candidate sources.

The electron density at the IF is the critical quantity for estimating the flux of ionizing photons striking the globule if we assume that the recombination rate roughly balances ionizations. From the ratio [S II] $\lambda6717 \div \lambda6731$ we find $n_e \simeq 2200$ cm^{-3} in the thin [S II] emitting region on the surface of the globule (see Table 3). However, this is only the value near position b, which may be somewhat unusual because of its nearly planar geometry, as noted earlier, and ground-based spatial resolution in these spectra does not effectively sample the highest density at the thin IF. At b and other positions a, c, d, and e, the electron density at the IF can be estimated independently using the extinction-corrected Hα surface brightness $S_{H\alpha}$ in Fig. 8. If we assume $n_e \simeq n_p$, and adopt a reasonable estimate of the depth of the emitting layer[3] along the line of sight L, then we have

$$n_e^2 = \frac{4\pi(S_{H\alpha} \times 206\,265^2)}{\alpha_{H\alpha}^{eff} h \nu_{H\alpha} L} \qquad (1)$$

where $\alpha_{H\alpha}^{eff} = 8.6 \times 10^{-14}$ cm^3 s^{-1} for $T \simeq 10^4$ K (Osterbrock 1989), and $206\,265^2$ just converts from arcsec^{-2} to sr^{-2} so that we can simply use values gleaned from Fig. 8. Adopted values of $S_{H\alpha}$, L, and n_e are listed in Table 4. Since n_e derived from images is somewhat higher than that derived from the [S II] lines for position b, as we would expect if [S II] lines trace a region where hydrogen already has a large neutral fraction, we take the values for n_e in Table 4

as more reliable estimates of the IF density. We can then use these values of n_e to estimate the number of ionizing photons Φ incident on an IF of radius r per second and per unit area if we assume that ionizations are approximately balanced by recombinations at the IF, so that we have

$$\Phi \simeq \Delta r \alpha_B n_e^2 \qquad (2)$$

where $\alpha_B = 2.59 \times 10^{-13}$ cm^3 s^{-1} is the total case B hydrogen recombination coefficient for $T \simeq 10^4$ K (Osterbrock 1989). To calculate Φ for the five positions listed in Table 4, we assumed the characteristic thickness of the recombination front is $\Delta r \simeq L \div 3$, which seemed a fair approximation based on the width of the limb-brightened surfaces seen in images. Judging by the morphology observed in Fig. 2, positions a through d all have the same ionizing source, and Table 4 indicates that all these positions have roughly the same incident flux of ionizing photons, with an average of $\log_{10}(\Phi) = 11.04$ s^{-1} cm^{-2}. Position e has a lower incident UV flux, with $\log_{10}(\Phi) \simeq 10.7$ s^{-1} cm^{-2}. The disagreement between the values of Φ for positions a through d compared to e is consistent with the apparent morphology in Fig. 2, where position e seems to have a different UV source.

The shape and relative intensities of various lines in Fig. 8 can also be used to constrain the spectral type of the ionizing star, by comparison to detailed emission models of photoevaporative flows. Sankrit & Hester (2000, SH hereafter) modelled ionized photoevaporative flows as seen in the same optical emission line tracers as we observed with *HST*. SH found that while the maximum density at the IF depends on the total ionizing flux but not on the shape of the incident continuum, the ratio of [O III] to Hα is sensitive to the spectral type of the ionizing star. In Table 4 we list spectral types of the ionizing stars inferred from values of the peak [O III]÷Hα ratio for positions a through e, corresponding to the models of SH with $\log_{10}(\Phi) \simeq 11$ s^{-1} cm^{-2} for positions a through d, and $\log_{10}(\Phi) \simeq 10.7$ s^{-1} cm^{-2} for position e (see their fig. 8). We regard these characteristic spectral types as very rough estimates; they should be taken as representing the approximate ratio of photons with $h\nu \gtrsim 35$ eV to those with $h\nu \gtrsim 13.6$ eV, rather than the actual spectral type of a main-sequence star (SH also noted that the derived properties differed depending on the type of model atmosphere used).[4] This is especially relevant to the possibility of WR25 as the ionizing source, as it is not a main-sequence star and has a strong wind ($\dot{M} = 10^{-4.4}$ M$_\odot$ yr^{-1}; Crowther et al. 1995). Also, these characteristic spectral types may underestimate the actual hardness of the source energy distribution, since hard photons may be absorbed in the ambient material between the star and the Finger or by dust in the photoevaporative flow itself. In general, the peak [O III]÷Hα ratios for positions a through d are consistent with a characteristic spectral type of ~O7 or O7.5, according to the models by SH, while position e requires a source with a spectral type later than B0 (an [O III] peak is weak or non-existent at position e).

Fig. 9 shows the hydrogen-ionizing photon luminosity $Q_H = 4\pi R^2 \Phi$ that would be required at a distance R to produce a flux of $\log_{10}(\Phi) = 11.04$ s^{-1} cm^{-2} at the surface of the Finger. This is compared to the actual values of Q_H and R for stars that are potential sources of the UV flux evaporating the Finger. Q_H values are taken from Smith, Norris & Crowther (2002) for the corresponding spectral type. For WR25 we adopted Q_H from the models by Crowther

---

[3] The values of L are determined from images in a somewhat subjective manner, and the uncertainties will be smallest for the ionization fronts at positions a and d, which have the least ambiguous geometry.

[4] When interpreting the characteristic spectral types, one should also keep in mind recent revisions to the T_{eff} scale for O stars (e.g. Martins, Schaerer & Hillier 2002).
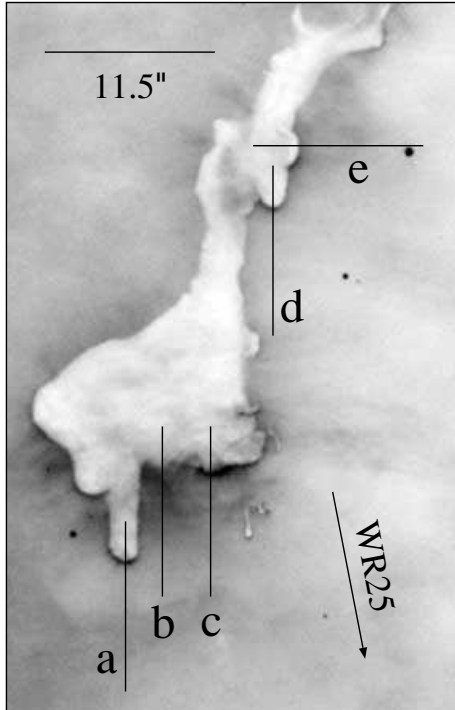
Figure 7. Locations of spatial intensity tracings superposed on the *HST*/WFPC2 F656N image of the Finger, rotated so that PA = 208° (the PA of the thin finger) is vertical. The positions labelled *a* through *e* correspond to tracings in Fig. 8.

Table 3. Parameters derived from dereddened line intensities.

Parameter	Units	IF	IBL	H II
n_e [S II]	cm^{-3}	2200 ± 500	860 ± 200	230 ± 70
T_e [N II]	K	9700 ± 400	9800 ± 400	12000 ± 400
T_e [O III]	K	9700 ± 700	10000 ± 700	15200 ± 1300
T_e [S III]	K	10000 ± 1500	8000 ± 1100	7200 ± 900

Values for TOT from lines in Table 2 are not shown here, because TOT contains distinct regions (IF and IBL) with different physical parameters.

Table 4. Ionization front properties.

Pos.	$S_{H\alpha}$ (^{a})	L (10^{16} cm)	n_e (cm^{-3})	$\log_{10}(\Phi)$ (s^{-1} cm^{-2})	Spectral Type^b
a...	6.5	3.5	6200	11.06	O7.5
b...	5.5	10.4	3300	10.99	O6.5
c...	7.0	6.9	4600	11.09	O7
d...	6.0	3.5	6000	11.03	O7.5
e...	3.0	10.4	2400	10.73	≲B0

^{a}10^{-13} erg s^{-1} cm^{-2} arcsec^{-2}. This Hα intensity may be contaminated somewhat by [N II] λ6583 included in the F656N filter; this effect is strongest at the IF. Using the [N II]/Hα ratio for the IF spectrum from Table 2, combined with the transmission curve of the F656N filter of HST/WFPC2, we estimate that [N II] contributes less than about 5 per cent of the measured Hα flux at the IF.
^{b}See Sankrit & Hester (2000).

et al. (1995; Crowther, private communication; models by Crowther et al. 1995 and Smith et al. 2002 include line blanketing.) The positions of these candidate source stars are identified in Fig. 1 and their properties are collected in Table 5. Fig. 9 shows two values for *R*: the separation on the sky given in Table 5, and a value that is a factor of

$\sqrt{2}$ larger to account for a possible projection effect. From Fig. 9 we conclude that the dominant source of ionization for the Finger is either the WNL star WR25 (Crowther et al. 1995) or the neighbouring O4 If star Tr16-244 (star number 257 of Massey & Johnson 1993) – or perhaps both working together. It is somewhat unsettling that the thin Finger appears to point toward a slightly skewed position angle of ∼208°, while WR25 is found at PA = 219° and Tr16-244 is at PA = 215°, relative to the Finger; one might expect a feature like the Finger to point *directly* toward its UV source. However, other factors may affect the appearance of photoionized columns as well (see Cantó et al. 1998; Williams et al. 2001). The Finger does point almost exactly at CPD −59°2574, but as an early B star, it does not even come close to providing the required ionizing flux (Fig. 9). Located directly south of the Finger, the massive hot stars HD 93204 and HD 93205 also provide insufficient ionization.

One further complication, however, is that the ionizing continuum striking the Finger appears to be softer than that produced by either WR25 or Tr16-244. The spectral type inferred from the [O III]÷Hα ratio at the IF is only about O7 (Table 4), whereas both likely UV sources have much earlier spectral types. We have not considered the effect of the strong X-ray flux from WR25 (e.g. Seward et al. 1979; Raassen et al. 2003). Since there are no other plausible sources of ionization in this direction, this suggests that the incident radiation field is softened as it passes through the nebula and the IBL on its way to the Finger. From the spectrum of the IBL we would derive an earlier spectral type from the [O III]÷Hα ratio than in the thin IF itself (Fig. 5 and Table 2).

5.3 Mass-loss rate and lifetime

From ^{12}CO(2-1) observations, Cox & Bronfman (1995) estimated a characteristic mass for the Finger of ∼6 M$_\odot$, but because the emission sampled mostly the warm surface of the cloud, they noted that the total mass of the globule is probably 10–20 M$_\odot$. This mass provides the reservoir for future photoevaporation, and allows us to estimate a likely evaporation time-scale for the cloud. If the evaporation of the cloud is dominated by the brightest southern IF, and if the geometry can be approximated as a cylinder illuminated on one side, the mass-loss rate is given roughly by

$$\dot{M} \simeq \pi r^2 m_H n_H v \qquad (3)$$

where *r* is the characteristic radius of curvature of the cloud appropriate for the apparent size of the IF (∼10$^{17.3}$ cm), and *v* is the speed of the evaporative flow through the IF. The electron density at the main evaporating surface (positions *c* and *d*) is ∼4000 cm^{-3} (Table 4), while right at the IF itself we typically have $n_e \simeq 0.7n_H$ because the gas is not fully ionized (e.g. SH). If we assume that the material expands away from the ionization front at the isothermal sound speed ($v \approx 10$ km s^{-1}), then $\dot{M} \approx 2 \times 10^{-5}$ M$_\odot$ yr^{-1}. In that case, the remaining lifetime of the entire cloud is 10$^{5.3}$–10^6 yr, about 7–30 per cent of the age of the nebula. The Finger and other associated molecular clumps probably represent the last vestiges of the original molecular cloud core that spawned Tr16, while significant reservoirs for future star formation exist in the neighbouring giant molecular cloud (Grabelsky et al. 1988).

6 STAR FORMATION IN THE FINGER?

In addition to the emission-line images described above, near-IR images in the *J*, *H* and *K* broad-band filters were obtained. A few reddened sources with $m_K \simeq 14$ were detected within the boundaries of the globule, but these were positioned randomly and could easily
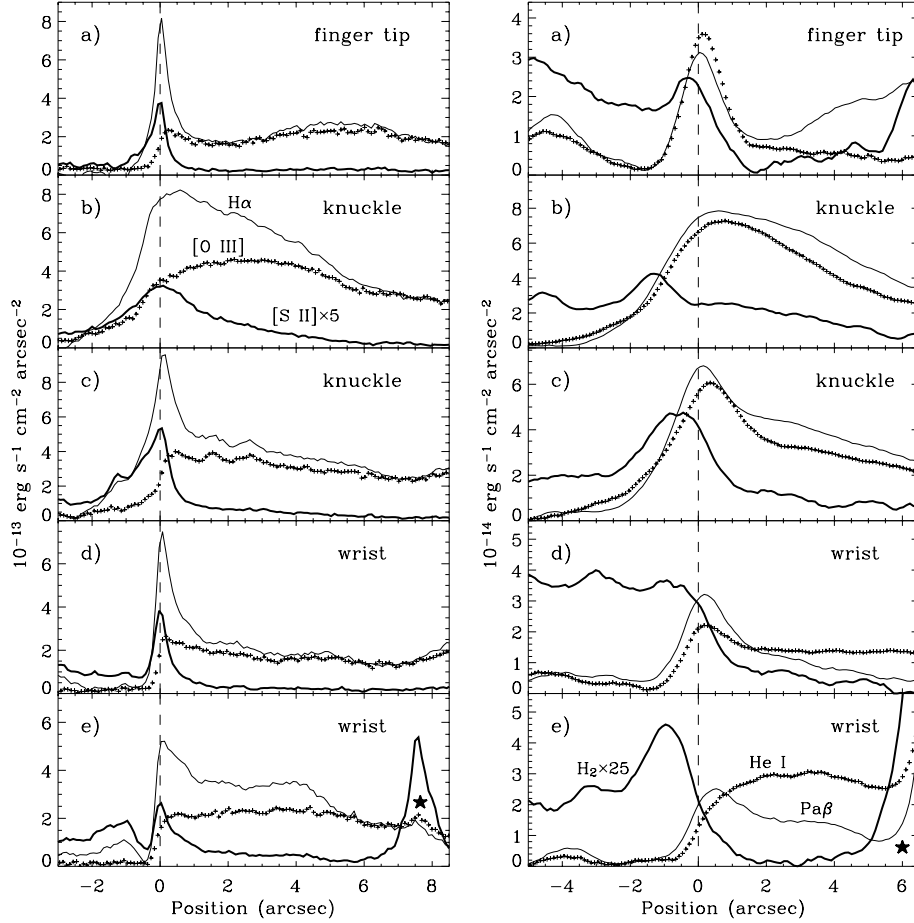
Figure 8. Intensity tracings of the ionization fronts and photoevaporative flows from the surface of the globule. Panels *a* through *e* correspond to the positions shown in Fig. 7. The left side shows intensity tracings made from *HST*/WFPC2 images in the [O III] λ5007 (F502N; crosses), Hα (F656N; thin line) and [S II] λλ6717+6731 (F673N; thick line) filters. The right shows tracings made from ground-based near-IR images in the light of He I λ10830 (crosses), hydrogen Paβ (thin line) and H₂ $v = 1 - 0$ S(1) λ21218 (thick line). All fluxes have been corrected for extinction and reddening with $E(B - V) = 0.37$ and $R = 4.8$, as shown in Fig. 6. In each filter, a constant value was subtracted corresponding to the emission from the background H II region far from the globule. Note that the weaker lines of [S II] and H₂ have been multiplied by factors of 5 and 25, respectively, for more effective comparison. The horizontal axis shows spatial position relative to the peak of the [S II] emission, adopted as the nominal location of the ionization front. The star symbol in panel (e) marks the position of a star (see Fig. 7).

be chance alignments of background sources (these point sources can be seen in the 2.122-μm H₂ image in Fig. 3c). A few of these *K*-band sources seem preferentially located near the limb-brightened edges of the globule, but no reddened stars were detected near the southern ionization front or inside the thin 'finger' protruding from it, as one might have expected. However, that does not necessarily mean that no stars are currently forming here or that no stars will form in the future. Below we estimate the amount of extinction in the Finger and the *K*-band source that could be hidden, as well as other pertinent quantities like the column density and mass in the Finger and its associated globule. Then we discuss implications for current and future star formation in this globule.

6.1 Extinction and dust mass

The Finger globule is seen as a silhouette in [O III], Hα, He I λ10830 and Paβ, so tracings through the globule in these emission lines can be used to estimate the optical depth, mass column density and total mass of the globule. Fig. 10 shows representative cross-cuts through the middle of the globule and through the thin finger (perpendicular to tracing *a* in Fig. 7). Differences in spatial resolution

between the *HST* and ground-based data aside, it is clear that the minimum emission intensity in the centre of each tracing I_λ increases with wavelength. Thus, the globule becomes translucent at the longer near-IR wavelengths. Interpreting these tracings is not entirely straightforward, however, because the Finger is not a simple silhouette blocking light from a background source – instead, it is a bright-rimmed globule suspended inside the H II region. Thus, some fraction of the observed minimum intensity originates along our line-of-sight to the Finger or near its surface. For example, it would not be unreasonable to assume that roughly half the intensity for each line in Fig. 10 is foreground emission. Since the globule has a flat-bottom profile and negligible limb brightening in [O III], we can make a crude correction for this foreground emission if we assume that the globule is optically thick and 'black' in the [O III] line. Then, the effective transmission at a given wavelength is given by $(I_\lambda - I_{O3})/(1 - I_{O3})$, where I_{O3} is the minimum flux in the [O III] line in the middle of the globule. Contamination from the IBL is probably worst in Hα and Paβ, so using the He I λ10830 line, we estimate an effective transmission through the middle of the globule of roughly 30 per cent, and a corresponding optical depth (τ) of ~1.2 at a wavelength of 1.08 μm. Similarly, for the thin finger
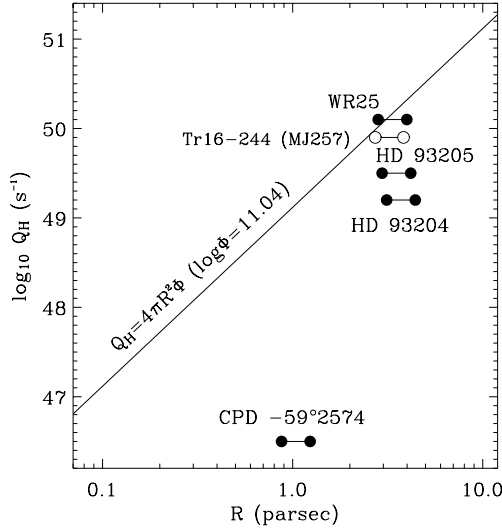
Figure 9. The solid line labelled $Q_H = 4\pi R^2 \Phi$ shows the number of hydrogen-ionizing photons Q_H that a star must emit at a separation R_{pc} in order to ionize the Finger. Q_H is plotted for several stars including WR25 at two different distances; the near distance is just the projected separation on the sky, and the far distance is an arbitrary factor of $\sqrt{2}$ larger.

Table 5. Candidate UV sources.

Star	Spectral type	PA (deg)	R (parsec)	$\log_{10}(Q_H)$ (s^{-1})
WR25	WNL	219	2.82	50.1
Tr16-244	O4 If	215	2.71	49.9
HD 93205	O3.5 V ((f))	176	2.96	49.5
HD 93204	O5 V ((f))	179	3.12	49.2
−59°2574	B1–B1.5 V	209	0.87	46.5

Spectral types are taken from Walborn et al. (2002) and Massey & Johnson (1993), R is the projected separation from the Finger measured in images, and ionizing photon fluxes for spectral types are taken from Smith et al. (2002), except for WR25 where Q_H is from models by Crowther et al. (1995). Also, HD 93205 is a binary, actually classified as O3.5 V ((f)) + O8 V, but the hotter component dominates the ionizing luminosity.

we estimate a slightly higher τ of $\sim$1.5 at 1.08 μm. The dust-mass column density is given by

$$m_{DUST} \simeq \frac{4a\rho\tau}{3Q_{abs}} \qquad (4)$$

where $a \approx 0.1$ μm is the assumed grain radius (large grains dominate the opacity), $\rho \approx 1$ g cm^{-3} is the average grain mass density, and $Q_{abs} = 0.04$ is the extinction coefficient at 1.08 μm (e.g. Draine & Lee 1984). Then, with $1.2 \lesssim \tau \lesssim 1.5$ at 1.08 μm, we have characteristic dust-mass column densities of 4 to 5×10^{-4} g cm^{-2}. If we integrate over the entire projected area of the globule, and assume a typical gas–dust mass ratio of 100:1 (this is the dominant source of uncertainty), then we find a total mass for the Finger globule of 6–8 M$_\odot$. Likewise, the mass of the small clump at the end of the thin finger is of order 0.1–0.2 M$_\odot$. The corresponding hydrogen column density through the globule is $N_H \approx 2$ to 3×10^{22} cm^{-2}.

The excellent agreement with the mass of 6 M$_\odot$ derived for the globule by Cox & Bronfman (1995) is fortuitous, given the large inherent uncertainty in the assumed gas–dust mass ratio. In fact, just as Cox & Bronfman noted that their value was an underestimate because the CO emission was dominated by warm outer layers of the globule, ours is probably an underestimate because some parts
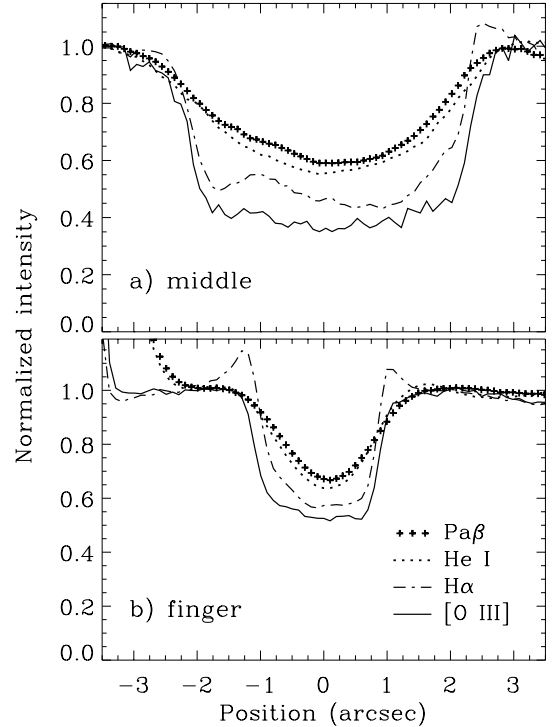

Figure 10. Normalized intensity cuts (a) through a narrow section near the middle of the globule and (b) through the thin extended finger for several emission lines. These tracings are useful for assessing the extinction in the globule (see text, Section 6.1).

of the finger may be optically thick even at 1–2 μm and may hide additional mass.

In our images, the K-band detection limit for point sources projected against the uneven background emission associated with the Finger globule is $m_K \simeq 17$. The extinction estimated above could then hide an intrinsic $m_K \simeq 15.5$ source from detection. At 2.3 kpc, this corresponds to an absolute K magnitude of roughly 3.5–4, or a young star of roughly 0.3–0.5 M$_\odot$. (Note that this is comparable to the minimum mass of dust and gas within the end of the thin finger.) Considering our detection limit we cannot rule out the possibility that a low-mass star has already formed at the end of the finger, so deeper *JHK* images with high spatial resolution are desirable.

6.2 Future star formation in the Finger?

Even though we have found no direct evidence for newly formed stars within the Finger, this globule and others like it in Carina may still be likely sites of future star formation. In Section 5.3 we found that the remaining lifetime before the globule evaporates away is of order $10^{5.3}$–10^6 yr, which is longer than the average free-fall time for the whole globule, and is plenty of time to allow a dense clump to collapse and form a protostar that would survive exposure to the interior of the H II region. Thus, it is worth a closer look at the physical conditions within the globule and its advancing IF. In particular, we ask whether the formation of a star may be triggered by radiation-driven implosion. We consider two cases: the main southern IF working on the body of the globule, and the end of the thin finger protruding from it.

6.2.1 The main ionization front

With a characteristic radius of $\sim$10 arcsec or $\sim 3 \times 10^{17}$ cm, the Jeans mass for the whole globule is $\sim$2 M$_\odot$ (T/10 K). Thus, with

a temperature of 10–40 K (e.g. Cox & Bronfman 1995), a mass larger than 6 $M_\odot$ makes it plausible that the globule can collapse to form stars – or at least, one could argue that the globule is on the verge of collapse under self-gravity, neglecting rotation and magnetic support. Thus, external pressure may play an important role in the future of the globule.

When evaluating if radiation-driven implosion is important, we must consider pressure balance between the ionization front (P_{if}) and the pressure inside the neutral globule (P_0). We have

$$P_{if} = n_e k T_e + m_H n_e v^2 \tag{5}$$

$$P_0 = \frac{\rho_0}{\mu m_H} kT + \rho_0 \sigma^2 + \frac{B^2}{8\pi} \tag{6}$$

where $m_H n_e v^2$ is the back-pressure from the photoevaporative flow launched from the IF (roughly equal to $n_e kT$), ρ_0 is the mass density, μ is the mean molecular weight, $\rho_0 \sigma^2$ is the inferred turbulent pressure of the molecular gas, and the last term in equation (6) is the magnetic pressure inside the cloud. The electron density and temperature of the IF are roughly 4000 cm^{-3} and 10^4 K (Tables 3 and 4), respectively, the average mass density ρ_0 inside the cloud is $\sim 2 \times 10^{-19}$ g cm^{-3} (see Section 6.1), and σ is roughly 1.1 km s^{-1} inferred from CO linewidths of 2.7 km s^{-1} (Cox & Bronfman 1995). If we neglect magnetic fields,[5] we find $P_{if}/P_0 \simeq 5$. Thus, a significant external overpressure may be causing the globule to collapse. If magnetic pressure is to support the globule, the perpendicular component of the magnetic field that would be required is $\sim 5 \times 10^{-4}$ G. Interestingly, in their analysis of the pillars of the Eagle Nebula, White et al. (1999) find a similar field of $B \simeq 5.4 \times 10^{-4}$ G (in fact, many of the physical parameters of the Finger resemble those estimated for the M16 pillars). However, as noted by those authors, a field of this strength would broaden the observed linewidth to $\gtrsim 4$ km s^{-1} because of Alfvénic motions, which is broader than the CO linewidth of 2.7 km s^{-1} reported by Cox & Bronfman (1995) for the Finger. Thus, we find it likely that radiation-driven implosion at the IF may be triggering the formation of low-mass stars in the globule.

6.2.2 The thin Finger

The thin finger protruding from the IF presents a somewhat different case, because it is smaller and denser than the main globule. One might expect that it was much denser than its initial surroundings, and that it has come into pressure equilibrium with the IF, since it has obviously resisted evaporation more than adjacent areas of the initial cloud (see also Williams et al. 2001). We approximate the end of the thin finger as a spherical globule with radius 5×10^{16} cm, a mass of $\gtrsim 0.2$ $M_\odot$ (see Section 6.1), and a corresponding mass density of $\sim 10^{-18}$ g cm^{-3}. The Jeans mass is then ~ 0.3 $M_\odot$ (T/10 K), and again we find it plausible that the dense clump may be in the process of collapsing to form a star – especially if 0.2 $M_\odot$ is an underestimate of the mass of the clump because of high optical depth as noted earlier. Following the analysis above, we find $P_{if}/P_0 \simeq 1.4$. This is considerably more uncertain than for the main globule above, because turbulence dominates the internal pressure, and we do not know to what extent the value of σ used above applies to the

small fingertip (this uncertainty also precludes a meaningful estimate of the magnetic field needed to halt collapse). Thus, the most likely scenario may be that the fingertip is in pressure equilibrium, and that a slowly advancing D-type (dense) IF is eating into the fingertip, and the shock from the IF has long ago passed through the clump. If a star is to form here, the process should already be underway. The fingertip may contain a faint low-mass protostar that has escaped detection in our images, or it may have a very young Class 0 protostar. In the latter case, thermal IR emission from a dense hot core would be difficult to detect, as it would be masked by thermal emission from the adjacent warm IF and PDR.

7 CONCLUSIONS

We have presented optical narrow-band *HST*/WFPC2 images, ground-based optical spectra, and near-IR images of the 'Finger' – a photoevaporating molecular globule in the core of the Carina Nebula. The main conclusions of this work are the following:

(i) The Finger globule exhibits an interesting morphology, with a thin extended middle finger apparently pointing toward its source of ionizing photons. The spatially resolved structure of the stratified ionization fronts are consistent with the interpretation of the Finger as an optically thick photoevaporating molecular globule, similar to structures often seen in *HST* images of H II regions.

(ii) Quantitatively, electron densities and the corresponding flux of ionizing photons incident upon the southward-facing ionization fronts of the Finger indicate that the dominant UV source is either WR25 (a late-type Wolf–Rayet star), Tr16-244 (O4 If), or perhaps both. This is reassuring, since the finger points to within a few degrees of these stars.

(iii) The mass-loss rate for the main evaporating surface of the globule is of order 2×10^{-5} $M_\odot$ yr^{-1}.

(iv) From extinction measurements, we estimate an average hydrogen column density of a few times 10^{22} cm^{-2} through the globule, and a total mass (assuming a gas–dust mass ratio of 100:1) of at least 6 $M_\odot$, in agreement with independent estimates from molecular studies. This is an underestimate if the globule contains clumps that are optically thick in the near-IR.

(v) The remaining lifetime of the globule before it is evaporated away is of order $10^{5.3}$–10^6 yr.

(vi) Several reddened stars are seen projected within the boundaries of the Finger globule, but whether or not these sources are newly formed stars that are physically associated with the globule is uncertain. No reddened star is seen at the apex of the thin protruding finger or immediately behind the main ionization front, down to a limit of $m_K \simeq 17$.

(vii) Considering the properties of the advancing ionization front, it appears likely that stars are currently forming or will soon form in the globule, triggered by radiation-driven implosion. At the main ionization front we find an external overpressure of a factor of ~ 5, and a smaller overpressure ($\gtrsim 1$) at the end of the thin finger.

---

[5] Note that turbulence dominates over thermal pressure, and we have neglected rotation because the straight edges of the thin finger protruding from the globule suggest that it has maintained the same orientation for its evaporation time-scale of 10^5 yr.

REFERENCES

Bertoldi F., 1989, ApJ, 346, 735
Bertoldi F., Draine B. T., 1996, ApJ, 458, 222
Bertoldi F., McKee C. F., 1990, ApJ, 354, 529
Bok B. J., Reilly E. F., 1947, ApJ, 105, 255
Brooks K. J., Burton M. G., Rathborne J. M., Ashley, M. C. B., Storey J. W. V., 2000, MNRAS, 319, 95
Cantó J., Raga A. C., Steffen W., Shapiro P. R., 1998, ApJ, 502, 695
Cardelli J. A., Clayton G. C., Mathis J. S., 1989, ApJ, 345, 245
Cox P., Bronfman L., 1995, A&A, 299, 583
Crowther P. A., Smith L. J., Hillier D. J., Schmutz W., 1995, A&A, 293, 427
Deharveng L., Maucherat M., 1975, A&A, 41, 27
Draine B. T., Lee H. M., 1984, ApJ, 285, 89
Dyson J. E., 1973, A&A, 27, 459
Dyson J. E., Williams R. J. R., Redman M. P., 1995, MNRAS, 227, 700
Elmegreen B. G., 1976, ApJ, 205, 405
Gorti U., Hollenbach D., 2002, ApJ, 573, 215
Grabelsky D. A., Cohen R. S., Bronfman L., Thaddeus P., 1988, ApJ, 331, 181
Hawarden T. G., Brand P. W. J. L., 1976, MNRAS, 175, 19
Herbig G. H., 1974, PASP, 86, 604
Hester J. J. et al., 1996, AJ, 111, 2349
Hummer D. G., Storey P. J., 1987, MNRAS, 224, 801
Kahn F. D., 1969, Physica, 41, 172
Lizano S., Canto J., Garay G., Hollenbach D., 1996, ApJ, 468, 739
López J. A., Meaburn J., 1984, Rev. Mex. Astron. Astrophys., 9, 119
Martins F., Schaerer D., Hillier D. J., 2002, A&A, 382, 999

Massey P., Johnson J., 1993, AJ, 105, 980
McCaughrean M. J., Andersen M., 2002, A&A, 389, 513
Oort J. H., Spitzer L., 1955, ApJ, 121, 6
Osterbrock D. E., 1989, Astrophysics of Gaseous Nebulae and Active Galactic Nuclei. University Science, Mill Valley
Raassen A. J. J., van der Hucht K. A., Mewe R., Antokhin I. I., Rauw G., Vreux J. M., Schmutz W., Güdel M., 2003, A&A, 402, 653
Rathborne J. M., Burton M. G., Brooks K. J., Cohen M., Ashley M. C. B., Storey J. W. V., 2002, MNRAS, 331, 85
Reipurth B., 1983, A&A, 17, 183
Reipurth B., Raga A., Heathcote S., 2003, AJ, 126, 1925
Sankrit R., Hester J. J., 2000, ApJ, 535, 847
Seward F. D., Forman W. R., Giacconi R., Griffiths R. E., Harnden F. R., Jr, Jones C., Pye J. P., 1979, ApJ, 234, L55
Smith L. J., Norris R. P. F., Crowther P. A., 2002, MNRAS, 337, 1309
Smith N., 2002, MNRAS, 331, 7
Smith N., Gehrz R. D., Krautter J., 1998, AJ, 116, 1332
Smith N., Bally J., Morse J. A., 2003a, ApJ, 587, L105
Smith N., Morse J. A., Bally J., Phelps R. L., 2003b, PASP, 115, 342
Smith N., Bally J., Brooks K. J., 2004, AJ, 127, 2793
Smith R. G., 1987, MNRAS, 277, 943
Thackeray A. D., 1950, MNRAS, 110, 529
Thompson R. I., Smith B. A., Hester J. J., 2002, ApJ, 570, 749
Walborn N. R., 1975, ApJ, 202, L129
Walborn N. R., 1995, Rev. Mex. Astron. Assoc. Ser. Conf., 2, 51
Walborn N. R. et al., 2002, AJ, 123, 2754
White G. J. et al., 1999, A&A, 342, 233
Williams R. J. R., 1999, MNRAS, 310, 789
Williams R. J. R., Ward-Thompson D., Whitworth A. P., 2001, MNRAS, 327, 788

This paper has been typeset from a T_EX/L^AT_EX file prepared by the author.